Materials & Design 212 (2021) 110200

Contents lists available at ScienceDirect

Materials & Design

journal homepage: www.elsevier.com/locate/matdes

Novel approach based on autoclave bead foaming to produce expanded polycarbonate (EPC) bead foams with microcellular structure and controlled crystallinity

Ismael Sánchez-Calderón [a,*], Victoria Bernardo [b], Judith Martín-de-León [a], Miguel Ángel Rodríguez-Pérez [a,c]

[a] Cellular Materials Laboratory (CellMat), Condensed Matter Physics Department, University of Valladolid, Campus Miguel Delibes, Paseo de Belén n°7, 47011 Valladolid, Spain
[b] CellMat Technologies S.L, Paseo de Belén 9-A, 47011 Valladolid, Spain
[c] BioEcoUVA Research Institute on Bioeconomy, University of Valladolid, 47011 Valladolid, Spain

HIGHLIGHTS

- Autoclave bead foaming methodology to produce expanded polycarbonate bead foams.
- The density of the expanded polycarbonate beads can be tuned through the saturation temperature.
- Crystallinity can be modified by controlling the saturation time without affecting the density and the cellular structure.
- Expanded polycarbonate bead foams with low density, micrometric cell size, and controlled crystallinity are obtained.
- Results make expanded polycarbonate produced by autoclave bead foaming a promising foam to the design of on-demand materials.

GRAPHICAL ABSTRACT

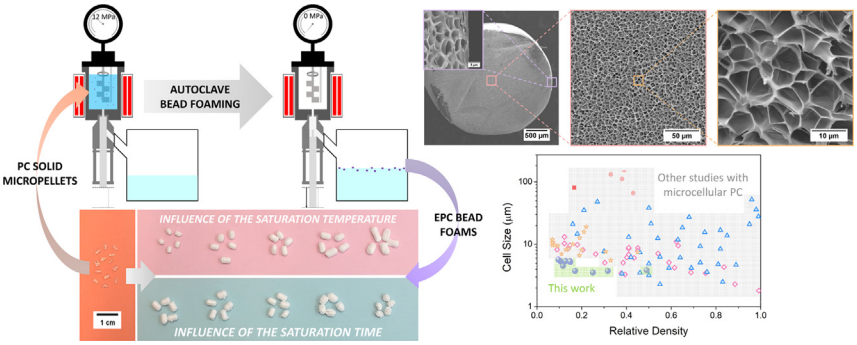

ARTICLE INFO

Article history:
Received 28 June 2021
Revised 10 September 2021
Accepted 26 October 2021

Keywords:
Bead foaming
Polycarbonate
Expanded polycarbonate
EPC
Crystallinity

ABSTRACT

Polycarbonate (PC) is a widely used engineering thermoplastic. Also, bead foaming technology is a method to produce high-performance, low-density foams with complex geometries. In this work, expanded polycarbonate (EPC) with microcellullar structure and low density have been produced for the first time using the autoclave bead foaming technique. The effect of the processing parameters, such as the saturation temperature and time, on the characteristics of the EPC bead foams, is analyzed. Contrary to the total amorphous structure of the solid material, the obtained EPC foams present a crystalline phase characterized by a melting peak around 235 °C. The crystallization process might be taking place during the saturation of the samples with CO_2. Results show that the saturation temperature allows controlling density, whereas foaming time can be used as a tool to control crystallinity degree in the range from 7.5 to 45 min, without a clear influence on the cellular structure. EPC with densities between 116 and 592 kg/m^3, cell sizes of approximately 4–5 µm, and crystallinities ranging 0–11% were produced by a proper modification of the foaming parameters. Then, the use of different saturation parameters allows controlling the density and thermal properties of the EPC, thanks to the autoclave bead foaming process.

* Corresponding author.
E-mail address: ismaelsc@fmc.uva.es (I. Sánchez-Calderón).

https://doi.org/10.1016/j.matdes.2021.110200
0264-1275/

1. Introduction

Polycarbonate (PC) is a well-known engineering thermoplastic, widely used in the industry for its versatile characteristics (high stiffness, impact strength, transparency, and thermal resistance), eco-friendly processing, and recyclability [1]. Due to its properties, one interesting application of PC is the production of lightweight, high-performance materials. In other words, to combine weight reduction with the good mechanical properties of the PC matrix. This could be achieved by producing PC foams using bead foaming technology.

Polymer foams can be manufactured via different technologies [2]. Within the possible production routes, one alternative that allows to generate low-density foams is the bead foaming technology [3]. Bead foaming consists of producing small beads that latter can be molded into complex parts by welding the beads. There are two routes to generate bead foams: the continuous process (using foam extrusion and an underwater pelletizer) and the batch process (using an autoclave). Either way, bead foaming is a very well-known technique for semi-crystalline polymers like polypropylene (PP) [4,5], poly(lactic acid) (PLA) [6,7], and thermoplastic polyurethane (TPU) [8,9]. It is also used to produce expanded polystyrene (EPS) [3]. The products generated by bead foaming are currently widely used in different sectors, such as the automotive industry (EPP), the insulation sector (EPS), the packaging sector (EPS and EPLA), or the sports industry (ETPU). Thanks to the combination of properties of bead foams, the interest to translate this technology to other foamed products has increased over the last years [10,11]. Recently, Weingart et al. [12] produced expanded polycarbonate (EPC). They foamed the beads by extrusion foaming and cut the foamed filament into beads by underwater pelletizing. The EPC beads foams showed a density of 200 kg/m^3 and a cell size of 81 μm. They reported enhanced mechanical properties of the EPC in comparison with commercially expanded polypropylene (EPP) and expanded polyethylene-terephthalate (EPET) at the same final density (200 kg/m^3), which become more pronounced as the temperature increases, showing the potential and advantages of the EPC. Up to date, this is the only work in which the generation of EPC is reported. As far as the authors know, there are no previous reports dealing with the fabrication of EPC foams in a batch set up using an autoclave.

The autoclave bead foaming process is similar to the solid-state gas dissolution foaming [13]. It consists of saturating polymer solid micropellets with a blowing agent at certain conditions of pressure, temperature, and time. The solid micropellets are dispersed in a medium (i.e., water) with surfactants in constant stirring to prevent sticking. After full saturation, pressure is abruptly released. If the saturation temperature is high enough, the solid micropellets expand during the depressurization (one-step process). Otherwise, a second foaming step must be applied to induce foaming (two-steps process). Autoclave bead foaming presents the advantage that cycle times are much shorter than in a gas dissolution foaming with large samples. Also, fast depressurization and expansion play an important role in this technique [3], leading to lower densities.

PC foaming via gas dissolution foaming has been widely investigated. Kumar et al. [14] reported the production of microcellular PC for the first time. They studied the influence of the saturation and foaming parameters in a two-step gas dissolution process. Densities ranging from 100 to 1200 kg/m^3 and cell sizes between 1 and 13 μm were obtained. Later, Weller et al. [15] further explore the production parameters to control the foam density and cell size to test the mechanical properties as a function of the cell size [16]. They extend the cell size range up to 50 μm and test the mechanical properties of foams with a fixed density of 670 kg/m^3 and cell sizes ranging between 3 and 37 μm, observing that mechanical properties were enhanced by reducing the cell size. While a unimodal cell-size distribution characterized the previous works, Ma et al. [17] tailored the production parameters to obtain bimodal structures to improve the mechanical properties. In the previous works, the saturation times typically ranged between 6 and 70 h for samples of 1.5 mm thickness. Another possibility to enhance the mechanical properties of PC foams is to increase the crystallinity [18,19]. During saturation, the CO_2 induces plasticization, decreasing the glass transition temperature (T_g) and allowing the foaming [20]. Besides, under some conditions, it also induces crystallization in PC [21]. Mascia et al. [22] studied the conditions leading to cells' formation and the onset of crystallization of bisphenol-A polycarbonate in a one-step process, varying the saturation conditions. Crystallinities as high as 24.3% were reported. They noticed that despite the presence of melting peaks in the first heating cycle, no recrystallization took place in the cooling cycle and that the vitrification temperature range remained constant. Also, Li et al. [23] studied the effects of saturation temperature and pressure on the crystallization kinetics and on the thermal behavior of crystallized PC. Both authors confirmed that CO_2-induced crystallization occurs during saturation. Finally, Gedler et al. [24] reported that the presence of the cellular structure and crystals enhanced the thermal stability of PC, which increases as the relative density of the samples decreases.

Given the already proved outstanding mechanical properties of the PC foams, the advantages of the autoclave bead foaming, and the interesting crystallization process that suffers the PC during the saturation, in this work, we studied, for the first time, the production of EPC by autoclave bead foaming. The effects of saturation temperature and time are investigated for a one-step foaming process. Density, cellular structure, and thermal properties of the produced EPC bead foams are characterized. EPC bead foams with low density, micrometric cell size, and controlled crystallinity are obtained. These results make EPC produced by autoclave bead foaming a promising foam to the design of on-demand materials.

2. Experimental

2.1. Materials

PC Lexan™ 105 (from Sabic) was used in this study. This material is a linear polycarbonate with a density of 1.2 g/cm^3 and a melt flow index of 7 g/10 min measured at 300 °C and 1.2 kg according to ASTM D1238. PC micropellets were obtained by extrusion using a twin-screw extruder model COLLIN TEACH-LINE ZK 25 T, with L/D of 24 and screw diameter of 25 mm. Before extrusion, the raw material was dried under vacuum at 70 °C for 12 h. The extruder temperature profile was from 225 to 270 °C (in the die), and the screw speed was 120 rpm. The produced material was cooled in a water bath and micro-pelletized. Extruded PC micropellets show a cylindrical shape with a diameter around 1 mm and 2 mm in height (see Fig. S1b of the Supplementary Information), a density (ρ) of 1.2 g/cm^3 and a glass transition temperature (T_g) of 150 °C.

Medical grade carbon dioxide (CO_2) (99.9% purity) was used as the blowing agent for the foaming experiments.

2.2. Autoclave bead foaming experiments

Foaming experiments were performed in a high-pressure stirred reactor (model PARR 4544) provided by Parr Instruments Company with a capacity of 600 ml, capable of operating at a maximum temperature of 350 °C and a maximum pressure of 34.5 MPa. The reactor is equipped with a magnetic stirrer, a thermocouple inside

the vessel, and a heater. A controller (Parr 4848 Reactor Controller) monitors both the stirring speed and the temperature. An accurate pressure pump controller (model SFT-10) provided by Supercritical Fluid Technologies Inc. automatically controls the CO_2 pressure to keep the desired value. The key feature of this equipment is the bottom drain valve that allows both depressurizing and extracting the micropellets from the reactor simultaneously.

This setup (Fig. 1) was used to produce the EPC bead foams with a batch foaming process. 4 g of PC micropellets were firstly introduced in the pressure vessel along with various surfactants (0.2 g of calcium stearate, 0.1 g of talc, and 1 g of sodium lauryl sulfate) in 440 ml of water. The mixture, under constant stirring, is then pressurized with CO_2 at 12 MPa of pressure to saturate the micropellets with the blowing agent. The time to reach the pressure and thermal stability is 30 min in all the experiments. Several experiments were conducted using the one-step approach varying the saturation temperature and time to investigate their effects on the microstructure of the EPC foams. For a fixed saturation time (30 min after reaching 12 MPa), the saturation temperature was varied between 150 and 170 °C in intervals of 5 °C. The saturation time effect was also studied by ranging this parameter between 7.5 and 60 min for a fixed saturation temperature (160 °C). After saturation, the pressure was abruptly released by opening the bottom drain valve, and the solid micropellets expanded into bead foams. The water/surfactants mixture with the samples was poured into an expansion tank filled with water at room temperature to cool down the EPC foams and stop the expansion. Pictures of the produced EPC bead foams are presented in Supplementary Information Section S1.

2.3. Characterization

2.3.1. Density

The solid micropellets density was measured with a gas pycnometer (model AccuPyc II 1340, Micromeritics). The density of the corresponding bead foams was determined with the water-displacement method based on Archimedes' principle with a density determination kit for an AT261 Mettler-Toledo balance. The volumetric expansion ratio (ER) is calculated as the ratio between the density of the solid and the density of the foam. The relative density (ρ_r) was also calculated as the ratio between the foam density and the solid density. The samples of this work present a solid skin on the surface that cannot be removed due to the small size of the samples. Then, density is measured with this solid skin. Fig. 2 shows an example of the solid skin of one of the samples produced in this work (12 MPa, 160 °C, and 30 min). As observed, the solid skin is very thin, with a thickness of approximately 1 μm. For all the materials produced in this work, this solid skin had a very low thickness (around 1 μm).

2.3.2. Cellular structure

The cellular structure of the samples was analyzed using a Scanning Electron Microscope (FlexSEM 1000 VP-SEM). The samples were fractured with a blade and coated with gold using a sputter coater (model SCD 005, Balzers Union). Several parameters were measured to obtain a complete analysis of the cellular structure. A tool based on the software ImageJ/FIJI [25] was used to quantify the structural parameters. The average cell size in 3D (ϕ_{3D}), the cell size distribution, and the standard deviation coefficient of the cell size distribution (SD) were obtained [25]. As an indicator of the homogeneity of the cellular structure, the parameter SD/ϕ_{3D} (normalized standard deviation coefficient) was calculated. Cell density (N_v) was determined using Kumar's theoretical approximation [26] according to Eq. (2), where A is the analyzed area and n is the number of cells in that area. Several beads were fractured to account for the possible heterogeneity between beads in the same batch, and more than 170 cells were analyzed for each material.

$$N_v = \left(\frac{n}{A}\right)^{3/2} \tag{2}$$

Also, the cell nucleation density (N_0) was determined using Eq. (3) using the relative density (ρ_r).

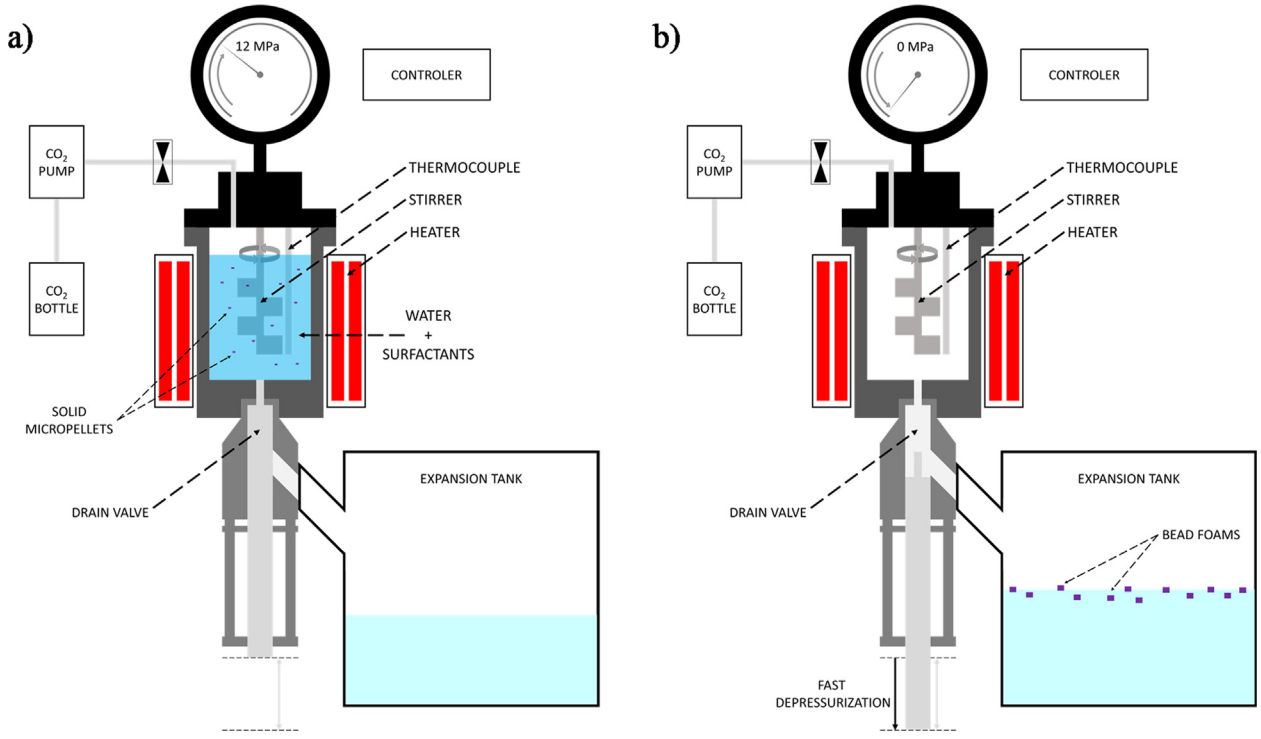

Fig. 1. Experimental setup scheme: a) saturation step and b) depressurization step.

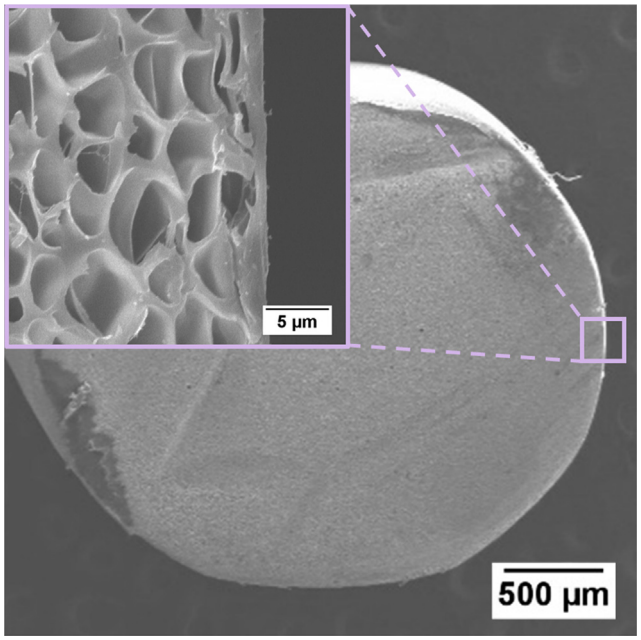

Fig. 2. Solid skin of the sample produced at 12 MPa, 160 °C, and 30 min.

$$N_0 = \frac{N_v}{\rho_r} \tag{3}$$

2.3.3. Thermal properties

The thermal properties were characterized by differential scanning calorimetry (DSC) (model DSC3+, Mettler). The program used was divided into three steps. First, a heating step from 30 °C to 250 °C at 20 °C/min. Second, a cooling step from 250° to 30 °C, at a rate of −20 °C/min. Finally, a heating step from 30 °C to 250 °C at 20 °C/min. The glass transition temperature (T_g) was taken as the mid-point of the DSC thermogram change that characterizes this transition and was calculated in both heating steps. Meanwhile, the melting point temperature (T_m) was taken as the temperature of the melting peak of the first heating step. The crystallinity (X_C) of the obtained EPC foams was estimated using Eq. (4). ΔH_m is the enthalpy of crystallization per gram of the sample, and $\Delta H_{m,0}$ the enthalpy of crystallization per gram of 100% crystalline PC. The latter was taken as 147.79 J/g [27].

$$X_C(\%) = \frac{\Delta H_m}{\Delta H_{m,0}} \cdot 100 \tag{4}$$

3. Results and discussion

3.1. Influence of the saturation temperature

The analysis of the influence of the saturation temperature was carried out using 12 MPa as saturation pressure and a saturation time of 30 min. Photographs of the EPC foams produced in this section can be found in Fig. S1b (Supplementary Information).

The evolution of the EPC bead foams density, cell size, and cell nucleation density as a function of the saturation temperature is shown in Fig. 3. Fig. 4 shows the cellular structure of the samples at different magnifications. On the one hand, as shown in Fig. 3a, the density of the beads is reduced as the saturation temperature increases, from 592 kg/m^3 at 150 °C to 126 kg/m^3 at 170 °C. The T_g of the solid PC is 150 °C, but the beads foamed at this temperature thanks to the plasticization effect of CO_2 that reduces the effective glass transition ($T_{g,eff}$). A reduction of at least 30 °C is expected, taking into account previous data [20,24]. The temperature gap between the $T_{g,eff}$ and the saturation temperature determines the expansion, and as the temperature increases, the temperature gap increases, allowing a higher expansion. Note that density reduction between 150 and 155 °C is higher than in the successive steps of increasing 5 °C (Fig. 2a). It can be due to two factors. First, the saturation temperature is too close to the $T_{g,eff}$, then the polymer's molecular chains have less movability, resulting in lower expansion. Second, as commented later, this material (the one produced at 150 °C) presents higher crystallinity (Fig. 5c). Crystallinity is a factor that also limits the expansion because crystals stiffen the material. Furthermore, since gas molecules cannot penetrate the crystals, the total amount of absorbed gas decrease as crystallinity increases, leading to higher $T_{g,eff}$. Both reasons could explain the low expansion obtained at 150 °C (ER of 2). Between 165 and 170 °C, the density seems to be constant with an ER of approximately 9.

On the other hand, the cellular structure is homogeneous, as seen in the SEM images (Fig. 4), characterized by micrometric cell sizes around 4–5 µm an SD/φ_{3D} between 0.4 and 0.6 (Fig. 3b). See Supplementary Information Section S2 for details about the cell size distributions (Fig. S2a). Meanwhile, cell nucleation density values around 10^{11} nuclei/cm^3 are obtained. It seems that 170 °C sets a limit since the density is not further reduced, and the structure shows some open cells (Fig. 4d.3). As the open cell content increases, the gas escapes quickly from de cells, limiting the expansion because there is no more pressure gradient promoting it. Notice that 126 kg/m^3 (obtained at 170 °C) is a very low density which combined with the cell size of 5 µm improves the data obtained in the literature for EPC bead foams (200 kg/m^3 and 81 µm) [12]. Also, results are comparable to those obtained by Kumar et al. [14] in solid-state foaming (100–1200 kg/m^3 and 1–13 µm), with a reduction of the cycle time and the possibility of producing complex-shape materials thanks to the bead foaming technology.

The PC is initially amorphous regarding the thermal properties, as observed in the DSC curve (Fig. 5a). However, during the saturation process with CO_2, the polymer suffers a recrystallization process, resulting in a melting peak that can be observed in the first heating of the DSC curve around 235 °C. This melting temperature of the EPC bead foams is similar to those obtained by previous authors [21–23]. Fig. 5a shows the first heating step of the DSC curve in which the melting peak appears and a zoom of the melting peak region. Fig. 5c presents the evolution of the melting point temperature and the crystallinity of the EPC beads as a function of the saturation temperature. On the one hand, as the saturation temperature increases, the EPC beads present the melting point at higher temperatures, reaching 238 °C at 170 °C (Fig. 5c). This dependence of the T_m with the processing parameters was already observed by Li et al. [23]. By saturating at higher temperatures, the generation of more perfect crystals is promoted. As the perfection of the crystals increases, the melting peak temperature rises [23].

Regarding the EPC beads crystallinity, it is reduced from 10.8 % at 150 °C to 1.5 % at 160 °C and then increases to 4.1 % at 170 °C. The behavior between 150 and 160 °C is the expected one. As the saturation temperature rises, the mobility of the molecular chains of the polymer increases, then it gets harder to form and grow crystals; in other words, the crystal growth rate decreases. As a result, higher temperatures lead to lower crystallinities for the same saturation time. However, from 160 to 170 °C, the trend is quite the opposite. To understand this unexpected result is necessary to think about a change in the crystal formation mechanism. Li et al. [23] studied the crystallization of PC under CO_2 pressure conditions in a temperature range from 140 to 180 °C. They observed that, under presumed heterogeneous nucleation conditions, the crystal growth changed from a 3D to a 1D configuration

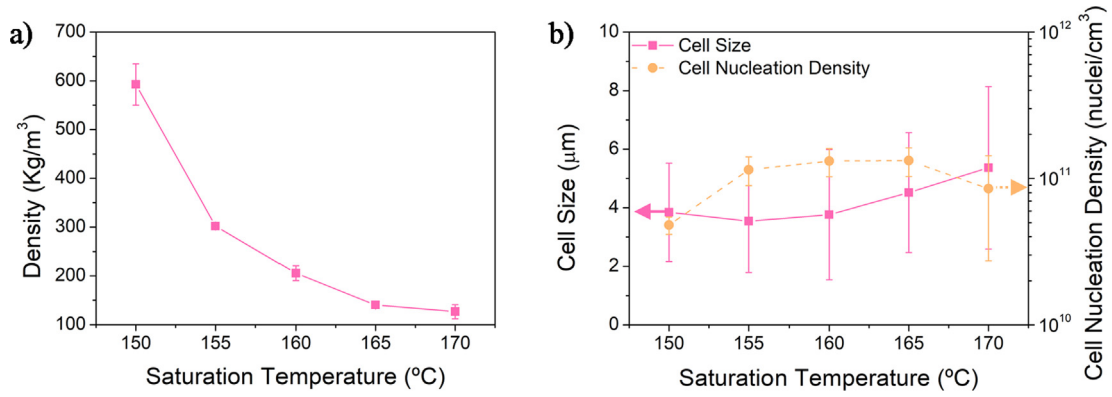

Fig. 3. a) Density and b) cell size (squares) and cell nucleation density (circles) of the EPC beads as a function of the saturation temperature. The bars of the cell size graph represent the standard deviation of the cell size distribution.

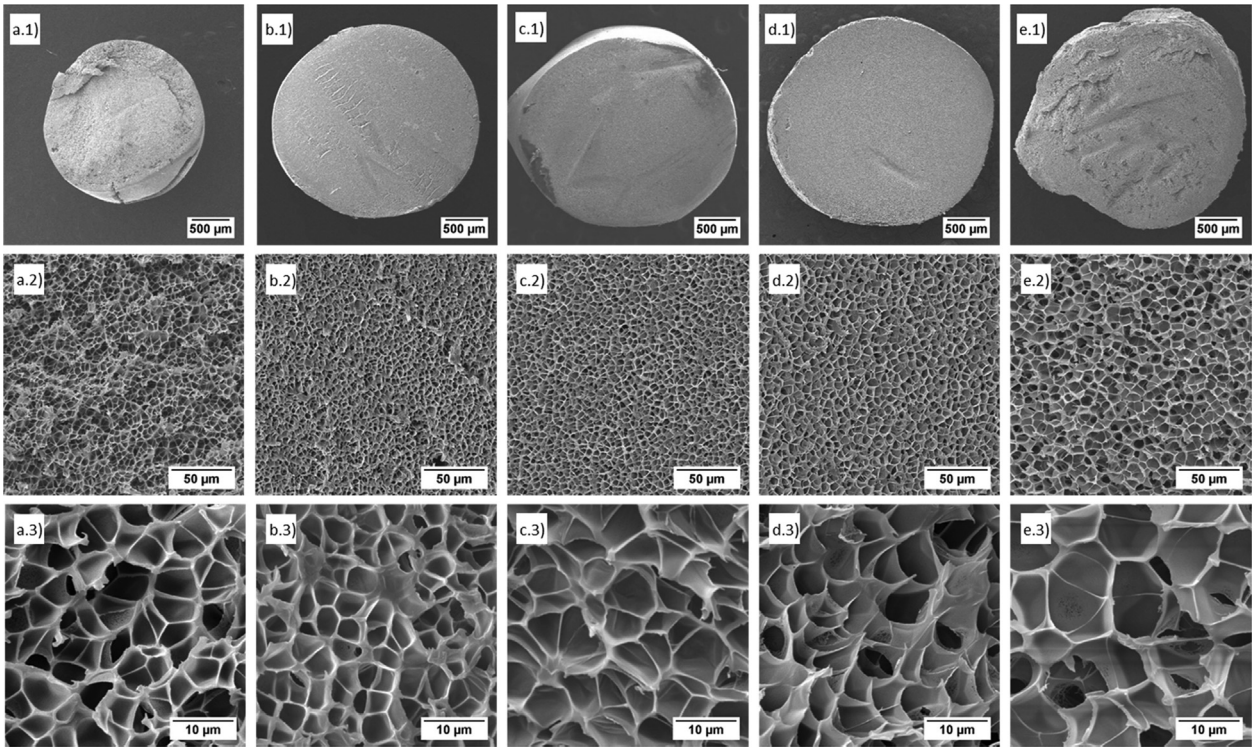

Fig. 4. SEM images of the EPC beads saturated at different temperatures at three different magnifications: a) 150 °C, b) 155 °C, c) 160 °C, d) 165 °C, and e) 170 °C. Fist row corresponds to low magnification, the second row to medium magnification, and the third row to high magnification images.

and that the crystal growth rate increases when the temperature was raised. Our hypothesis to explain the obtained results is that between 160 and 170 °C, the crystal grow configuration may be changing as proposed in the work of Li et al. [23], affecting the form and growth rate of the crystals. As a result of that changes, the degree of crystallinity (number or crystals and/or crystals size) is larger at 170 °C than at 165 °C and 160 °C for a fixed saturation time of 30 min.

In the first heating step, the material's glass transition temperature is reduced compared to the original material (Fig. 5d). This effect might be related to the presence of the cellular structure and the new microstructure of the PC crystals. The next stage of the DSC curve is the cooling step. Up to precision, no crystallization peak is observed in the cooling step. The third part of the cycle is the last heating. Once the second heating step is performed, the melting point disappears, and the T_g is still lower than that of the original (solid PC). Therefore, the T_g reduction is a permanent effect. Fig. 5b shows the second heating step of the DSC curve and a zoom of the glass transition region to better appreciation. The T_g of the second heating step is also shown in Fig. 5d. It is observed that the T_g is permanently reduced in comparison with the initial solid. Note that the glass transition of the solid PC is 150 °C. For example, at 160 °C, the T_g after the second heating step reaches 138 °C, which is a reduction of 12 °C in comparison to the solid PC. As mentioned before, this is a permanent change of the polymer. It is important to remark that the tendency between the evolution of the glass transition and the crystallinity is the opposite (as the glass transition increases, the crystallinity is reduced, and the other way around). The higher the crystallinity, the lower T_g.

One possibility that may explain this T_g permanent reduction is due to the high T_g of the solid PC (i.e., the strong molecular inter-

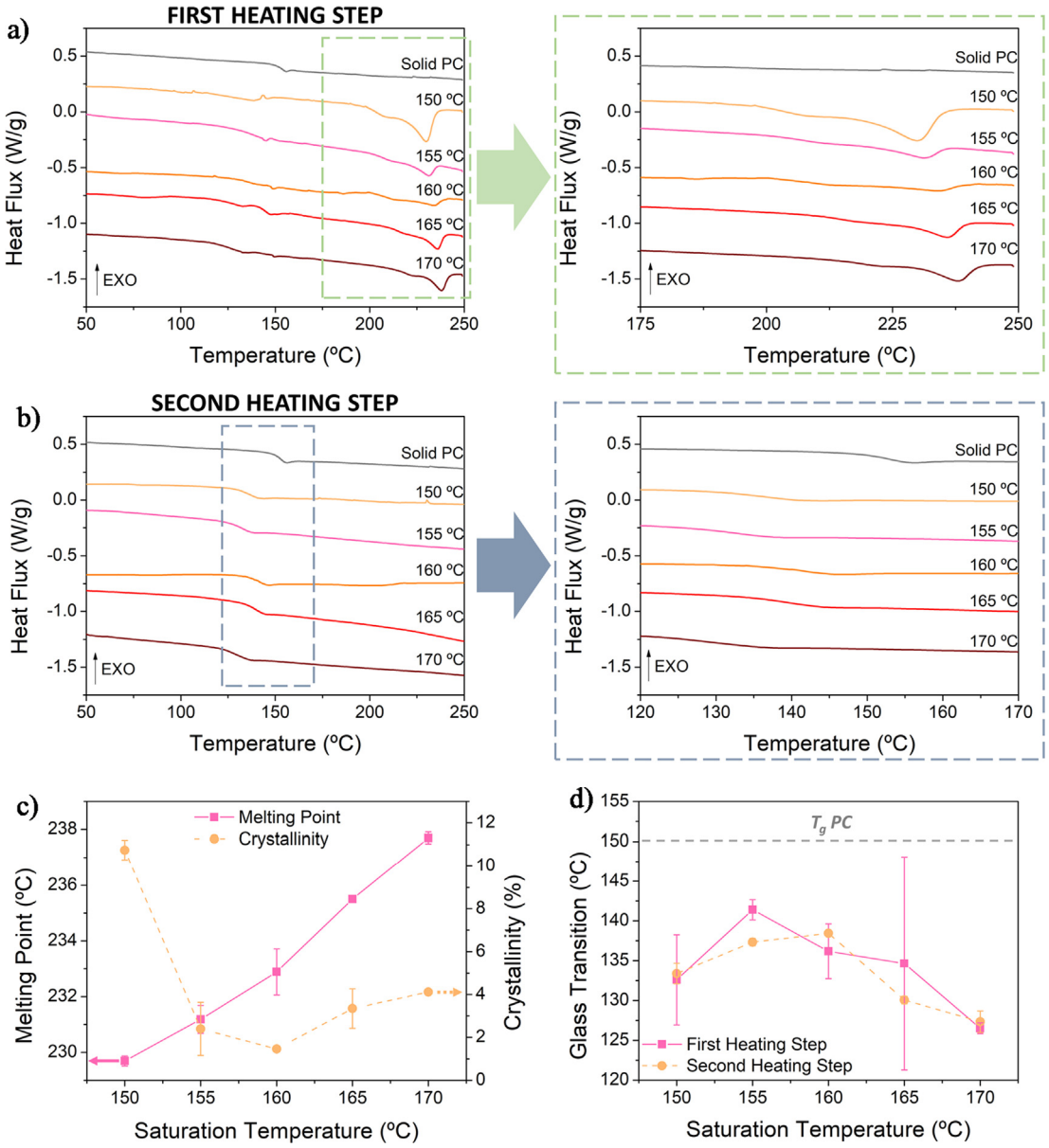

Fig. 5. DSC results of the EPC bead foams produced at saturation conditions of 120 bar, 30 min, and different temperatures: a) DSC curve of the first heating step with a zoom of the melting point region; b) DSC curve of the second heating step with a zoom of the glass transition region; c) melting point temperature (squares) and crystallinity (circles) as a function of the saturation temperature; and d) glass transition temperature in the first (squares) and second (circles) heating steps as a function of the saturation temperature.

actions of the PC). When plasticizing with CO_2, the molecular interactions are reduced, leading to a decrease in the T_g. Note that the EPC bead foams did not have CO_2 in the matrix I when they were measured by DSC. So, although the CO_2 promotes the T_g reduction during the PC foaming (allowing it), it is not the cause of its reduction once foamed. Once the PC is foamed, the T_g is lower, indicating that the structure of the amorphous phase has changed, not recovering the molecular interactions of the PC resin used in the study [28]. In fact, the initial molecular interactions are not recovered even when raising the temperature, being the reduction of T_g permanent, and probably because the necessary energy to modify the structure is too high. Therefore, the CO_2 can modify the amorphous phase structure permanently, and the structure is not recovered because the energy gap to achieve it is not overcome. Another possibility would be that we are degrading the polymer's molecular chains during the process, which can cause a permanent decrease of the T_g [29]. In particular, as no authors previously reported this effect, we suppose it may occur during the fast depressurization/-foaming and depends on the crystallinity degree achieved during the saturation.

3.2. Influence of the saturation time

The study of the influence of the saturation time was carried out employing 12 MPa and 160 °C as saturation parameters. A picture of the EPC foams can be found in Fig. S1c (Supplementary Information).

Fig. 6 shows the evolution of the EPC beads density (Fig. 6a) and cell size and cell nucleation density (Fig. 6b) as a function of the saturation time. Fig. 7 shows the cellular structure of PC bead foams saturated at 160 °C and different saturation times. As shown in Fig. 6a, the beads' density is almost constant between 7.5 and

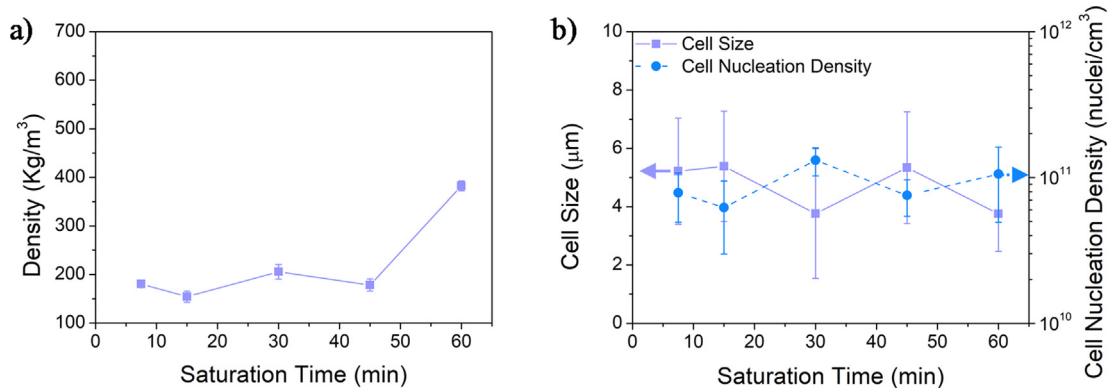

Fig. 6. a) Density and b) cell size (squares) and cell nucleation density (circles) of the EPC beads as a function of the saturation time.

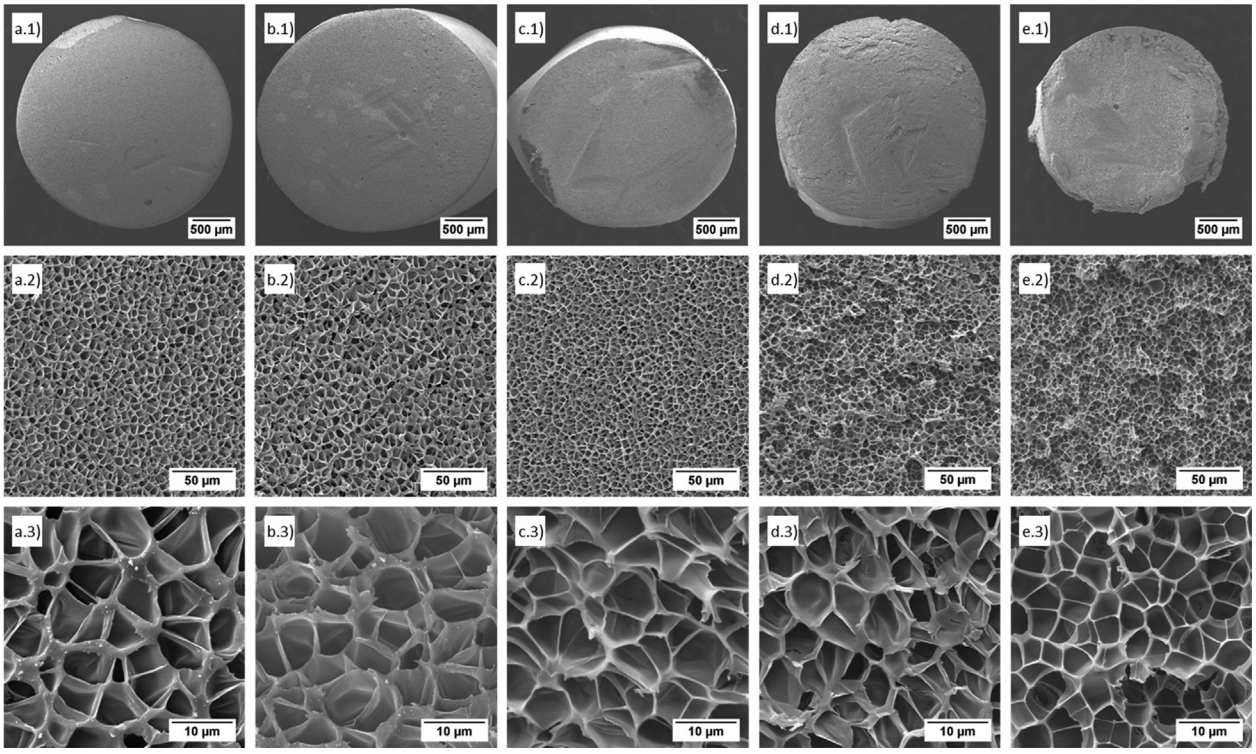

Fig. 7. SEM images of the EPC beads produced at different times at three different magnifications: a) 7.5 min, b) 15 min, c) 30 min, d) 45 min, and e) 60 min. Fist row corresponds to low magnification, the second row to medium magnification, and the third row to high magnification images.

45 min (around 180 kg/m^3, which means an ER of 6.6). At 60 min, the density increases, reaching 382 kg/m^3, probably due to the higher crystallinity of the material. As previously commented, crystallinity is a factor that limits expansion. Therefore, there is a critical value of crystallinity from which the expansion is limited. The cellular structure seems to not depend on the saturation time strongly (Fig. 7), being homogeneous (SD/φ_{3D} lower than 0.6) and taking values of cell size between 4 and 5 μm (Fig. 6b). Again, the cell nucleation density is almost constant (around 10^{11} nuclei/cm^3). As the saturation step is performed at the same temperature, initially, samples have the potential to absorb almost an equivalent quantity of CO_2, leading to the generation of the same number of nucleation points when the pressure is released. But, as the saturation time increases, the grade of crystallinity will increase (see Fig. 8c), which may reduce the amount of gas that can be absorbed. Note that given the standard deviation of the measurements, the cell sizes and cell nucleation densities are almost constant at the different saturation times. See Supplementary Information Section S2 for details about the cell size distributions.

Regarding the thermal properties, Fig. 8a shows the first heating step of the DSC curve in which the melting peak appears and a zoom of the melting peak region. In Fig. 8c, the melting point temperature and the degree of crystallinity evolution of the EPC beads as a function of the saturation time are presented. At 7.5 min, no melting peak can be observed; therefore, no crystallinity is induced at this temperature, or it is so small that it cannot be appreciated with the DSC. As the saturation time increases, the melting point temperature and the crystallinity of the EPC beads increase, reaching 235 °C and 11.1% at 60 min, respectively. On the one hand, the melting point temperature increase is associated with the perfection of the crystals. As the saturation time increases, the time that the CO_2 is plasticizing the material increases. It gives the chain molecules of the polymer more movability to reorganize and form

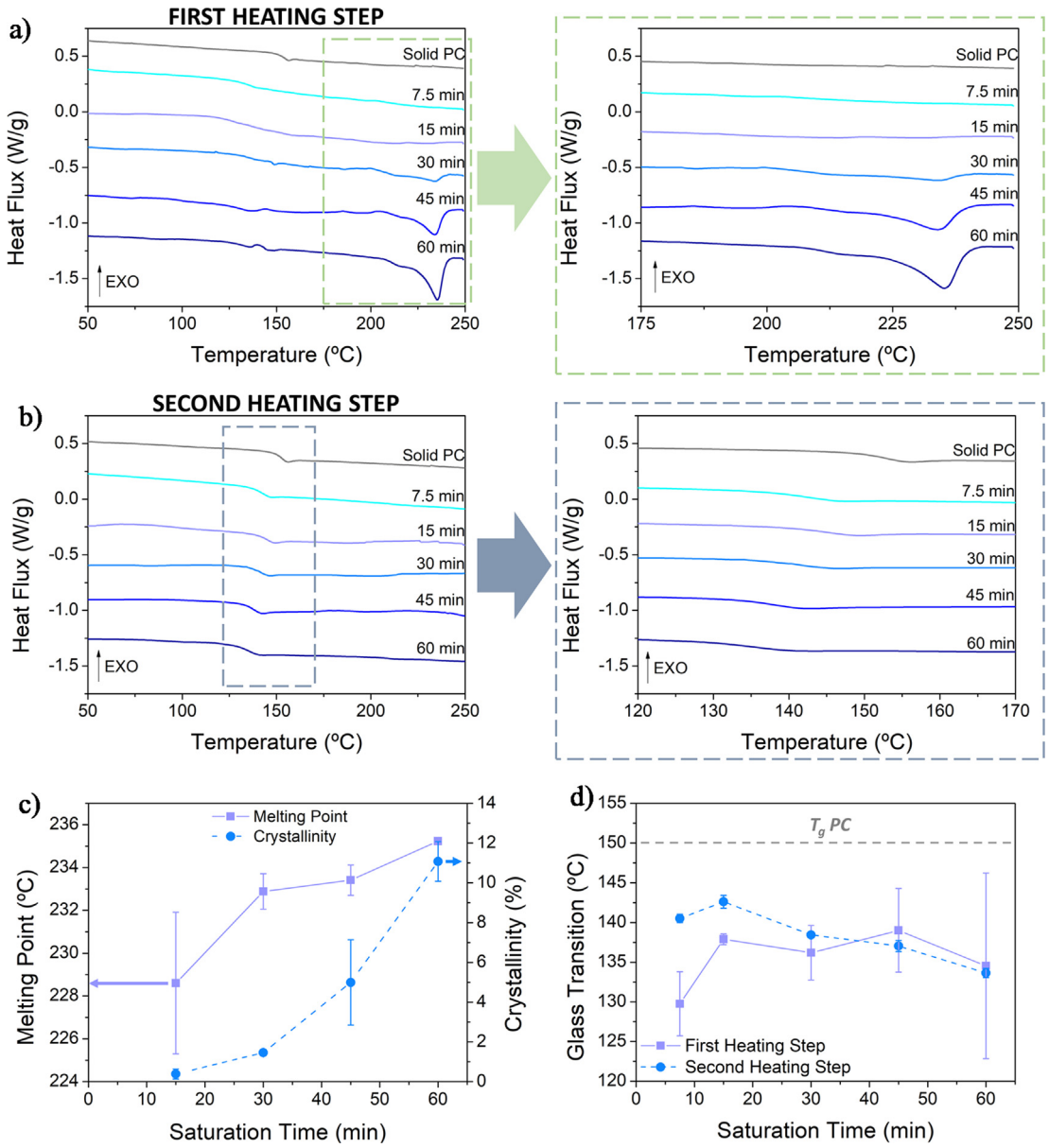

Fig. 8. DSC results of the EPC bead foams produced at saturation conditions of 120 bar, 160 °C, and different times: a) DSC curve of the first heating step with a zoom of the melting point region; b) DSC curve of the second heating step with a zoom of the glass transition region; c) melting point temperature (squares) and crystallinity (circles) as a function of the saturation time; and d) glass transition temperature in the first (squares) and second (circles) heating steps as a function of the saturation time.

crystals. On the other hand, the crystallinity rise is due to an increment of the size of the crystals because they have more time to grow. Again, the glass transition temperature appears displaced with respect to the original (solid PC) in the first heating cycle (Fig. 8d), probably due to the presence of the cellular structure and the new microstructure of the PC crystals. Once the second heating step is performed, the melting point disappears, but the T_g continues displaced (Fig. 8b). Fig. 8d shows the evolution of the glass transition temperature of the EPC beads with the saturation time on both heating steps. In the second heating step, as the saturation time increases, the T_g decreases from 142 to 133 °C between 15 and 60 min. Note that as the glass transition temperature decrease, the crystallinity increases, following the trend commented in the previous section. Despite the absence of crystallinity when saturated during 7.5 min, the EPC beads present the T_g depression. As commented before, it may be due to a change in the structure of the amorphous phase or due to degradation of the polymer's molecular chains during the fast depressurization/foaming.

Nonetheless, the saturation time variation leads to a crystallinity rise while maintaining the density and the cell size until a threshold is reached. This threshold is related to crystallinity, which limits expansion. Therefore, the control of the saturation time allows producing EPC bead foams with constant density and cell size and variable crystallinity.

3.3. EPC production optimization

As previously discussed, as the saturation temperature increases (from 150 °C to 170 °C) for a fixed saturation time (30 min), the density of the EPC bead foams decreases from 592 kg/m^3 to values as low as 126 kg/m^3. However, the beads obtained at 170 °C present an open cell cellular structure, which may be a cause that limits the expansion because the gas escapes

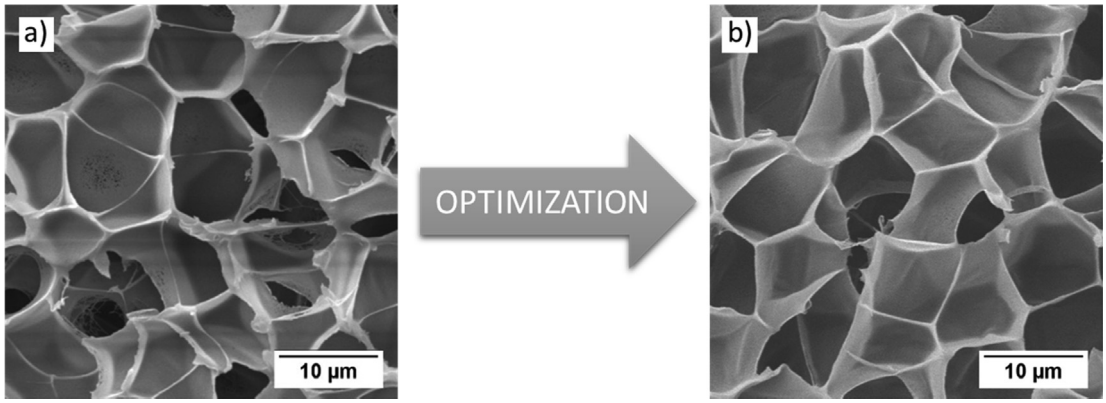

Fig. 9. High magnification SEM images of the EPC beads produced at a) 12 MPa 170 °C 30 min, and b) 12 MPa 170 °C 15 min.

Table 1
Comparison between the cellular and thermal properties EPC beads produced at 12 MPa, 170 °C, and 30 min and the EPC beads produced at 12 MPa, 170 °C, and 15 min.

	Density (kg/m^3)	Cell Size (μm)	Cell Nucleation Density (nuclei/cm^3)	Melting Point (°C)	Crystallinity (%)	Glass Transition (°C)
12 MPa 170 °C 30 min	126 ± 14	5.4 ± 2.8	$(8.5 \pm 5.8)\cdot10^{10}$	238	4.1	126 / 127
12 MPa 170 °C 15 min	116 ± 18	5.7 ± 2.2	$(8.6 \pm 2.5)\cdot10^{10}$	225	0.6	126 / 136

quickly from de cells. Furthermore, it was observed that as the saturation time increases, crystallinity and melting point temperature increase because the molecular chains have more time to reorganize, allowing a larger crystallization. As crystallinity limits the possible expansion, this effect leads to a threshold under which the density remains constant and above which density raises. For instance, the grade of crystallinity of the EPC bead foams produced at 160 °C increases from 0 to 5% between 7.5 and 45 min of saturation time, being the density almost constant (around 180 kg/m^3). In both cases (saturation temperature and time increase), the cell size is constant (4–5 μm).

Taking all this into account and in order to confirm the tuneability of the EPC bead foams, an additional experiment at 12 MPa and 170 °C has been performed. In this case, the saturation time has been reduced from 30 to 15 min. As shown in Table 1 (where the cellular and thermal properties of those foams are included), reducing the saturation time leads to a density reduction (from 126 to 116 kg/m^3) probably caused by the closed-cell structure of the foam produced at 15 min (Fig. 9). The cell size and cell nucleation density are similar (around 5.5 μm and $8.5\cdot10^{10}$ nuclei/cm^3, respectively). Furthermore, as expected, the melting point temperature moves to lower temperatures, and the grade of crystallinity is reduced (from 4.1 to 0.6%). This reduction of the degree of crystallinity could be one of the reasons for allowing the production of foams with a closed-cell structure and, as a consequence, a lower density.

3.4. Comparison with PC foams produced with CO_2 by other foaming routes

Finally, Fig. 10 presents a cell size versus relative density map to compare the produced EPC bead foams with PC foams produced with CO_2 by other foaming routes (gas dissolution foaming and extrusion bead foaming). It is observed that the EPC bead foams produced in this work fill a new region presenting the lowest cell size - relative density combination. Therefore, the foaming approach used in this research allows reducing density and cell size compared to the results obtained by gas dissolution foaming

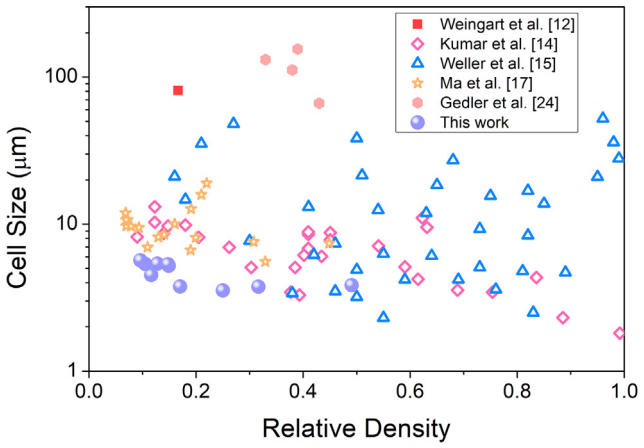

Fig. 10. Cell size - relative density map, including the results of this research and those previously published for microcellular PC foams fabricated by gas dissolution foaming and extrusion bead foaming.

[14,15,17,24], probably due to the own advantages of the autoclave bead foaming technique. On the one hand, the saturation of small micropellets dispersed in water enhances the heat transmission and reduces the cycle time. On the other hand, the fast depressurization allows obtaining enhanced cellular structures and reduced densities. The EPC bead foams produced in this work also improve the previous results obtained by extrusion bead foaming (Weingart et al. [12]. Note that they reported enhanced mechanical properties of an EPC (which lack of crystallinity) in comparison with commercial EPP and EPET. Therefore, given the crystallinity of the EPC produced by autoclave bead foaming, a rise in the mechanical properties can be expected.

4. Conclusions

Bead foams based on PC have been produced by means of an autoclave bead foaming process for the first time. The density,

cellular structure, and thermal properties of the obtained EPC bead foams have been studied as a function of the saturation temperature and time. Contrary to the total amorphous behavior of the solid material, the obtained EPC foams present some degree of crystallinity characterized by a melting peak around 235 °C. Therefore, the PC suffers a recrystallization process during saturation. As the saturation temperature or time increases, the melting point moves to higher temperatures, which means that the perfection of the crystals is increasing.

The morphology of the produced EPC bead foams is characterized by a solid skin of around 1 μm and an inner homogeneous cellular structure of cell sizes between 4 and 5 μm. The density of the EPC beads can be tuned through the saturation temperature in the range from 116 to 592 kg/m^3, while the crystallinity can be modified by controlling the saturation time. Thus, the proposed method allows the production of EPC beads foams with controlled characteristics. In comparison with other PC foams produced with CO_2, the EPC bead foams of this research show a unique cellular structure with high expansion (*ER* = 10) in combination with microcellular cell sizes.

Declaration of Competing Interest

The authors declare that they have no known competing financial interests or personal relationships that could have appeared to influence the work reported in this paper.

Acknowledgements

Financial support from the Junta of Castile and Leon grant (I. Sánchez-Calderón) is gratefully acknowledged. Financial assistance from the Spanish Ministry of Science, Innovation, and Universities (RTI2018-098749-B-I00 and PTQ2019-010560 (Victoria Bernardo-García)) and from EREN (Ente Regional de la Energía de Castilla y León EREN_2019_L4_UVA) are gratefully acknowledged.

Appendix A. Supplementary material

Supplementary data to this article can be found online at https://doi.org/10.1016/j.matdes.2021.110200.

References

[1] Z.Q. Liu, A.M. Cunha, X.-S. Yi, A.C. Bernardo, Key properties to understand the performance of polycarbonate reprocessed by injection molding, J. Appl. Polym. Sci. 77 (2000) 1393–1400, https://doi.org/10.1002/1097-4628(20000808)77:6<1393::AID-APP27>3.0.CO;2-4.

[2] F.L. Jin, M. Zhao, M. Park, S.J. Park, Recent trends of foaming in polymer processing: A review, Polymers (Basel). 11 (2019), https://doi.org/10.3390/polym11060953.

[3] D. Raps, N. Hossieny, C.B. Park, V. Altstädt, Past and present developments in polymer bead foams and bead foaming technology, Polymer (Guildf). 56 (2015) 5–19, https://doi.org/10.1016/j.polymer.2014.10.078.

[4] P. Guo, Y. Liu, Y. Xu, M. Lu, S. Zhang, T. Liu, Effects of saturation temperature/pressure on melting behavior and cell structure of expanded polypropylene bead, J. Cell. Plast. 50 (2014) 321–335, https://doi.org/10.1177/0021955X14525798.

[5] B.K. Jang, M.H. Kim, O.O. Park, Effects of Crystallinity and Molecular Weight on the Melting Behavior and Cell Morphology of Expanded Polypropylene in Bead Foam Manufacturing, Macromol. Res. 28 (2020) 343–350, https://doi.org/10.1007/s13233-020-8042-z.

[6] L. Tang, W. Zhai, W. Zheng, Autoclave preparation of expanded polypropylene/poly(lactic acid) blend bead foams with a batch foaming process, J. Cell. Plast. 47 (2011) 429–446, https://doi.org/10.1177/0021955X11406004.

[7] M. Nofar, A. Ameli, C.B. Park, Development of polylactide bead foams with double crystal melting peaks, Polymer (Guildf). 69 (2015) 83–94, https://doi.org/10.1016/j.polymer.2015.05.048.

[8] D. Zhao, G. Wang, M. Wang, Investigation of the effect of foaming process parameters on expanded thermoplastic polyurethane bead foams properties using response surface methodology, J. Appl. Polym. Sci. 135 (2018) 1–11, https://doi.org/10.1002/app.46327.

[9] T. Zhang, S.J. Lee, Y.H. Yoo, K.H. Park, H.J. Kang, Compression molding of thermoplastic polyurethane foam sheets with beads expanded by supercritical co2 foaming, Polymers (Basel). 13 (2021) 1–15, https://doi.org/10.3390/polym13040656.

[10] Q. Wang, J. Yang, P. Liu, L. Li, Facile One-Step Approach to Manufacture Environmentally Friendly Poly(vinyl alcohol) Bead Foam Products, Ind. Eng. Chem. Res. 60 (2021) 2962–2970, https://doi.org/10.1021/acs.iecr.1c00203.

[11] J. Jiang, W. Feng, D. Zhao, W. Zhai, Poly(ether imide)/Epoxy Foam Composites with a Microcellular Structure and Ultralow Density: Bead Foam Fabrication, Compression Molding, Mechanical Properties, Thermal Stability, and Flame-Retardant Properties, ACS Omega. 5 (2020) 25784–25797, https://doi.org/10.1021/acsomega.0c03072.

[12] N. Weingart, D. Raps, J. Kuhnigk, A. Klein, V. Altstädt, Expanded polycarbonate (Epc)—a new generation of high-temperature engineering bead foams, Polymers (Basel). 12 (2020) 1–19, https://doi.org/10.3390/polym12102314.

[13] V. Kumar, N.P. Suh, A process for making microcellular thermoplastic parts, Polym. Eng. Sci. 30 (1990) 1323–1329, https://doi.org/10.1002/pen.760302010.

[14] V. Kumar, J. Weller, Production of microcellular polycarbonate using carbon dioxide for bubble nucleation, J. Manuf. Sci. Eng. Trans. ASME. 116 (1994) 413–420, https://doi.org/10.1115/1.2902122.

[15] J.E. Weller, V. Kumar, Solid-State Microcellular Polycarbonate Foams. I. The Steady-State Process Space Using Subcritical Carbon Dioxide, Polym. Eng. Sci. (2010), https://doi.org/10.1002/pen.

[16] J.E. Weller, V. Kumar, Solid-state microcellular polycarbonate foams. II. The effect of cell size on tensile properties, Polym. Eng. Sci. 50 (2010) 2170–2175, https://doi.org/10.1002/pen.21737.

[17] Z. Ma, G. Zhang, Q. Yang, X. Shi, A. Shi, Fabrication of microcellular polycarbonate foams with unimodal or bimodal cell-size distributions using supercritical carbon dioxide as a blowing agent, J. Cell. Plast. 50 (2014) 55–79, https://doi.org/10.1177/0021955X13503849.

[18] A. Kumar, B. Patham, S. Mohanty, S.K. Nayak, Polypropylene–nano-silica nanocomposite foams: mechanisms underlying foamability, and foam microstructure, crystallinity and mechanical properties, Polym. Int. 69 (2020) 373–386, https://doi.org/10.1002/pi.5959.

[19] S. Yao, D. Hu, Z. Xi, T. Liu, Z. Xu, L. Zhao, Effect of crystallization on tensile mechanical properties of PET foam: Experiment and model prediction, Polym. Test. 90 (2020), https://doi.org/10.1016/j.polymertesting.2020.106649 106649.

[20] M.R. Holl, J.L. Garbini, W.R. Murray, V. Kumar, A steady-state mass balance model of the polycarbonate-CO2 system reveals a self-regulating cell growth mechanism in the solid-state microcellular process, J. Polym. Sci. Part B Polym. Phys. 39 (2001) 868–880, https://doi.org/10.1002/polb.1061.

[21] E. Beckman, R.S. Porter, Crystallization of bisphenol a polycarbonate induced by supercritical carbon dioxide, J. Polym. Sci. Part B Polym. Phys. 25 (1987) 1511–1517, https://doi.org/10.1002/polb.1987.090250713.

[22] L. Mascia, G. Del Re, P.P. Ponti, S. Bologna, G. Di Giacomo, B. Haworth, Crystallization Effects on Autoclave Foaming of Polycarbonate Using Supercritical Carbon Dioxide, Adv. Polym. Technol. 25 (2006) 225–235. https://doi.org/10.1002/adv.

[23] G. Li, C.B. Park, A New Crystallization Kinetics Study of Polycarbonate Under High-Pressure Carbon Dioxide and Various Crystallinization Temperatures by Using Magnetic Suspension Balance, J. Appl. Polym. Sci. (2010), https://doi.org/10.1002/app.

[24] G. Gedler, M. Antunes, V. Realinho, J.I. Velasco, Characterization Of Polycarbonate Foam Structure Prepared By One-Step SC-CO2 Dissolution Process, in: 10th Int. Conf. Foam Mater. Technol. Barcelona, Spain, 2012.

[25] J. Pinto, E. Solórzano, M.A. Rodriguez-Perez, J.A. de Saja, Characterization of the cellular structure based on user-interactive image analysis procedures, J. Cell. Plast. 49 (2013) 555–575, https://doi.org/10.1177/0021955X13503847.

[26] V. Kumar, Process synthesis for manufacturing microcellular thermoplastic parts, Massachusetts Inst. Technol., 1988.

[27] J. Brandrup, E.H. Immergut, Polymer Handbook, 2nd ed., Wiley, New York, 1975.

[28] D.R. Rueda, M.C.G. Gutiérrez, F.J.B. Calleja, S. Piccarolo, Order in the Amorphous State of Poly(ethylene terephthalate) as revealed by Microhardness: Creep Behaviour and Physical Ageing, Int. J. Polym. Mater. 51 (2002) 897–908.

[29] D. Huang, Y. Yang, G. Zhuang, B. Li, Influence of entanglements on the glass transition and structural relaxation behaviors of macromolecules. 1. Polycarbonate, Macromolecules. 32 (1999) 6675–6678, https://doi.org/10.1021/ma990581g.